Detection Method of Series Arc Fault in Three-Phase Frequency Converter Load Circuit Under Unknown Working Conditions

Hongxin Gao, *Member, IEEE*, Kunyuan Wang, Zhiyong Wang, *Member, IEEE*, Jiacheng Cai, and Yuze Lv

***Abstract*—Accurately detecting the series arc fault (SAF) in power lines and realizing the protection of the circuit are of great significance for effectively preventing electrical fire accidents. However, existing research results are difficult to effectively detect SAF that occurred in three-phase frequency converter load circuit under unknown working conditions. To solve the above problems, a new approach for SAF detection based on real-time training, updating prediction models and predicting residuals was proposed in this article. First, a prediction model based on dung beetle optimization algorithm optimized extreme learning machine was proposed. Second, SAF experiments in three-phase frequency converter load circuit were carried out under commercial power supply condition. The model was trained and updated by using two cycle current signals, so as to predict the next cycle current signal. The SAF detection was realized by combining the mean square error of the prediction residual and a threshold. Finally, the detection performance of the proposed method was tested under three unknown working conditions, which are different power harmonics, operating parameters of the frequency converter, and operating current, respectively. The results indicated that the proposed method can effectively detect the SAF occurred in the frequency converter load circuit under three unknown working conditions.**

***Index Terms*—Dung beetle optimization (DBO), extreme learning machine (ELM), fault detection, prediction model, series arc fault (SAF).**

I. Introduction

IN THE industrial field, a large number of three-phase frequency converters are used to control three-phase motors. The connecting cables and electrical connectors are often affected by external forces, such as vibration, dragging, or squeezing during the operation of the motor. In this case, it will cause problems, such as cable breakage, loose electrical connectors, and other problems, which will cause series arc fault (SAF). The SAF is accompanied by a high temperature above 4000 °C, which is much higher than the ignition points of combustible materials, such as cable insulation. The SAF is one of the main causes of electrical fire. The complex and variable working conditions of three-phase frequency converters in industrial field are one of the important reasons that restrict the development of the SAF detection technology. Therefore, it is of great significance to study a detection method for the SAF in three-phase frequency converter load circuit that can be applied to various unknown working conditions.

Applying current or voltage signals to detect the SAF is currently a research hotspot. He et al. [1] extracted the absolute average, harmonic amplitude, and wavelet energy entropy of the current signals, and used the feature thresholds to identify the SAF. Zhang et al. [2] first obtained the difference value of two adjacent current waveforms, then extracted the amplitude features after the wavelet threshold denoising, and used a given threshold to identify the SAF. Artale et al. [3] calculated the frequency spectrum between 0 and 500 Hz of current signals by using chirp-z transform, and then calculated a set of low-frequency characteristic indicators, and the thresholds and related limits-of-variation values were used to detect the SAF. Zhao et al. [4] first calculated the proportional coefficient of zero current time of the current signal and the maximum correlation coefficient of the improved normalized absolute values, then they were fused by a fuzzy logic processor and used as the fault features, and the thresholds were used to identify the SAF. Qu et al. [5] proposed a sparse representation method on the basis of the L_p norm with an online adjustable regular order, and the residual comparison and projection coefficient ratio were used to detect the SAF. Jiang and Zheng [6] reconstructed the coupled high-frequency differential signal by using spectral features, and combined Chebyshev distance with high-order center distance to detect the SAF. Lezama et al. [7] used the derivative of the inter-period autocorrelation coefficient of the line current as the fault feature, and adopted the threshold value to detect the SAF. Kim et al. [8] first performed infinite impulse response filtering on the voltage signal, then extracted the energy of the signal within the feature frequency band, and finally applied the threshold to detect the SAF. Calderon-Mendoza et al. [9] obtained two steady-state variables from the current signal by using Kalman filter, extracted residual and third-order difference as the fault features, and used a fuzzy logic processor to detect the SAF. Siegel et al. [10] took Fourier coefficients, Mel-frequency Cepstrum data and wavelet features of current signals as fault features, and utilized a deep neural network to detect the SAF.

Manuscript received 25 October 2023; revised 26 January 2024 and 24 March 2024; accepted 8 April 2024. Date of publication 12 April 2024; date of current version 16 May 2024. This work was supported by the National Natural Science Foundation of China under Grant 52077158. Recommended for publication by Associate Editor G.-S. Seo. *(Corresponding author: Hongxin Gao.)*

The authors are with the Faculty of Electrical and Control Engineering, Liaoning Technical University, Huludao 125105, China (e-mail: gaohongxin@lntu.edu.cn).

Color versions of one or more figures in this article are available at https://doi.org/10.1109/TPEL.2024.3387755.

Digital Object Identifier 10.1109/TPEL.2024.3387755

Ferracuti et al. [11] constructed the gray image from the current signals, extracted the texture features of gray co-occurrence matrix images, and used linear discriminant analysis to detect the SAF. Wang et al. [12] utilized sparse encoding to capture arc fault features in current signals, and combined it with fully connected neural networks to detect the SAF. Zhang et al. [13] adopted complete ensemble empirical mode decomposition and Hilbert transform to extract the fault features, and used a long short-term memory network (LSTM) to identify the SAF. Wang et al. [14] applied the raw current signal as the input features of a convolutional neural network (CNN), and developed an ArcNet model to detect the SAF. Wang et al. [15] extracted the time-domain and frequency-domain features of the current signal, divided the loads into three categories according to the feature parameters, and used a fully connected neural network to identify the SAF. Yu et al. [16] utilized a parallel deep CNN model to identify the SAF in low-voltage ac system. Jiang et al. [17] collected coupled high-frequency differential signals and expanded the sample data by using an improved *R–L–C* arc model, and used a one-dimensional CNN model to identify the SAF. Ding et al. [18] used the amplitude of the absolute difference between adjacent waves of the current signal to determine the starting period of the fault, and combined it with a one-dimensional CNN to identify the random features of the arc and detect the SAF. Gong et al. [19] used Pearson correlation coefficient to calculate the similarity between current cycles, solved the first-order derivative, and combined it with the AlexNet model to detect the SAF. Wang et al. [20] calculated the empirical wavelet transform (EWT) complex entropy and time-domain sensitive features of current signals, and performed fusion dimensionality reduction by using principal component analysis, and adopted a probabilistic neural network to achieve SAF detection. Rocha et al. [21] analyzed the power of the detailing signals of the wavelet decomposition of the current signals, and used a support vector machine (SVM) to detect the SAF. Gupta et al. [22] extracted the fault features by performing empirical mode decomposition on the current signals, and utilized a SVM to detect the SAF. Duan et al. [23] extracted the time domain and frequency domain features from the current signals, and applied the zero phase component analysis whitening transformation to reduce the correlation and redundancy of those features, and then adopted a broad learning system to detect the SAF. Han et al. [24] used the kurtosis and skewness of the fifth and sixth principal components of two current signals and a voltage signal as the fault features of the SAF, and utilized a SVM to identify the fault. Gao et al. [25] performed a five-layer decomposition on the current signal by using EWT, extracted the singular values of the improved attractor trajectory matrix for each decomposition signal as the fault features, and used a SVM to identify the SAF. Wang et al. [26] proposed a lightweight SAF identification model based on CNN, and developed an online detection device for the SAF by using the embedded device Jetson nano. Wang et al. [27] decomposed the current signal by using variational modal decomposition (VMD), extracted sample entropy and energy entropy as the fault features, and utilized a SVM to identify the SAF. Liu et al. [28] proposed a fault feature extraction method based on improved recurrence quantification analysis, and adopted a back-propagation (BP) neural network to detect

The above research results have achieved good performance in detecting the SAF under corresponding experimental conditions. They have played a positive role in promoting the development of theory and technology for SAF detection. However, there are still the following issues.

1) In [1], [2], [3], [4], [5], [6], [7], [8], [9], the SAF fault features were directly extracted from current or voltage signals, and the threshold method was used to detect the SAF. This method does not rely on a large amount of experimental data and only uses a small amount of experimental data to set the threshold. However, the power quality of the power supply, the operating status of the frequency converter and other working conditions can affect the current signal, leading to the changes of the extracted fault features. In this case, it is difficult to use threshold method to detect the SAF under different working conditions.
2) In [10], [11], [12], [13], [14], [15], [16], [17], [18], [19], [20], [21], [22], [23], [24], [25], [26], [27], [28], the supervised recognition methods, such as SVM and neural networks were used to detect the SAF. These methods require extensive arc fault experimental data to train the recognition models and rely heavily on label information. However, the working conditions in industrial field are very complex and variable, and the number of fault samples under actual field conditions is too small to cover unknown conditions. Establishing recognition models based solely on data under limited experimental conditions can only accurately classify samples under the same or similar conditions, making it difficult to detect the SAF under unknown working conditions.
3) The methods proposed in [1], [2], [3], [4], [5], [6], [7], [8], [9], [10], [11], [12], [13], [14], [15], [16], [17], [18], [19], [20], [21], [22], [23] are mainly aimed at the civilian field. The power supply, load type, and environmental conditions used in the civilian field are significantly different from those in industrial field. Therefore, the proposed methods are difficult to directly apply in the industrial field.

In response to the above issues, a SAF detection method based on the prediction residuals of model by using dung beetle optimization algorithm optimized extreme learning machine (DBO-ELM) was proposed. In the normal working circuit under different working conditions, although there are obvious differences in the current signal, the unpredictability in the current signal is weak. The predicted model residuals under different working conditions can be reduced by using real-time data to train the prediction model. When a SAF occurs in the circuit, due to the strong randomness and instability of the SAF, the unpredictability of the current signal in the fault state is enhanced. In this case, even if real-time fault data are used to train the model, the predicted model residuals will still be large. Therefore, it is easier to achieve a unified threshold under different working conditions. The main innovations and academic contributions of this article are as follows.

1) A new approach for detecting the SAF based on real-time training and updating prediction models was proposed to address the issue of no effective solution for detecting the SAF under unknown working conditions. It has certain

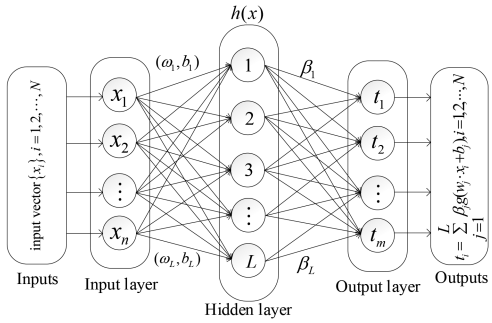

Fig. 1. Network structure of ELM.

reference value for detecting the SAF under unknown working conditions, unknown circuit topologies, unknown loads, and other conditions.

2) A SAF detection method based on the current predicted residuals of the DBO-ELM prediction model and a fixed threshold was presented. It can provide reference for the development of industrial arc fault circuit interrupters (AFCI) under unknown working conditions.

The rest of this article is organized as follows. Section II provides a detailed introduction to the basic theory and implementation steps of the DBO-ELM prediction model. Section III introduces the experimental platform and scheme of the SAF, and provides the implementation process and results of the detection method. Section IV presents the test results on the applicability of the proposed method under different power harmonics, frequency converter operating parameters, and current conditions. It also compares the detection performance of four existing SAF detection methods under unknown working conditions. Finally, Section V concludes this article.

II. DBO-ELM Prediction Model

In the field of data prediction, prediction models, such as BP neural network [29], support vector machine regression (SVR) [30], CNN [31] and LSTM [32] have been widely used. The idea of the SAF detection used in this article is that the prediction model needs to be retrained at each detection. The training speed of the prediction model directly determines the real-time performance of the SAF detection. Extreme learning machine (ELM) is a fast-learning algorithm, which is used to train single hidden layer feedforward neural networks. Compared with the methods, such as BP neural network and CNN, ELM generates the input weight and the hidden layer bias randomly, and calculates the output weigh through generalized inverse matrix, and the training process does not need iteration. So ELM has fewer training parameters and faster training speed [33], which is more suitable for the prediction model in this article. Besides, in order to improve the predictive performance of the ELM prediction model, the DBO algorithm was introduced to optimize the parameters of ELM.

A. ELM Theory

The network structure of ELM is shown in Fig. 1, which mainly includes input layer, hidden layer and output layer. The connection from the input layer to the hidden layer is fully connected.

If there are N arbitrary training samples $(x_i, t_i), i = 1, \cdots, N$. Where, $t_i = [t_{i1}, t_{i2}, \cdots, t_{im}]^T \in R^m$, $x_i = [x_{i1}, x_{i2}, \cdots, x_{in}]^T \in R^n$, x_i is an N-dimensional training sample. The output of the neural network with L hidden neurons and activation function $g(.)$ can be represented as

$$t_i = \sum_{j=1}^{L} \beta_j g(w_j \cdot x_i + b_j), i = 1, 2, \cdots, N \tag{1}$$

where, b_j is the bias of the jth hidden layer neuron. w_j is the weight that connects the jth hidden layer neuron with the input neurons, $w_j = [w_{j1}, w_{j2}, \cdots, w_{jn}]^T$. β_j is the output weight of the jth hidden layer neuron, $\beta_j = [\beta_{j1}, \beta_{j2}, \cdots, \beta_{jm}]^T$.

The matrix expression of formula (1) is as follows:

$$H\beta = T \tag{2}$$

where H is the output matrix of the hidden layer, and its formula is expressed as

$$H(w_1, w_2, \cdots, w_L, b_1, b_2, \cdots, b_L, x_1, x_2, \cdots, x_N) = \begin{pmatrix} g(w_1 x_1 + b_1) & \cdots & g(w_L \mathrm{x}_1 + b_L) \\ \vdots & \ddots & \vdots \\ g(w_1 x_N + b_1) & \cdots & g(w_L x_N + b_L) \end{pmatrix} \tag{3}$$

where β is the output weight that connects hidden layer neurons and output neurons

$$\beta = H^+ T \tag{4}$$

where T is the expected output matrix, $T = [t_1, t_2, \cdots, t_m]^T$. $H^+$is the Moore-Penrose generalized inverse matrix of the matrix H.

B. DBO-ELM Model

When the ELM is trained each time, it randomly selects the input weight and the hidden layer bias. It will cause the change of the output weight, and then make the prediction residual fluctuate. This is not conducive to the unification of the fault determination thresholds. To improve the prediction accuracy and stability of the prediction model, it is necessary to optimize the input weight and hidden layer bias of ELM. Since the input layer and the hidden layer of ELM algorithm are fully connected, there are a large number of input weights and hidden layer bias that need to be optimized. The DBO algorithm is an optimization algorithm based on bionics principle. It has the advantages of simplicity and high computational efficiency. It is suitable for large-scale optimization problems [34]. So, the DBO algorithm was introduced to optimize the input weight and hidden layer bias of ELM.

The DBO algorithm simulates the group behavior and cooperation mechanism of dung beetles. It consists of multiple dung beetle individuals that communicate and transmit information through foraging behavior and mutual attraction. The algorithm balances the local and global search ability by the updating rules of four behaviors, i.e., rolling, breeding, foraging and stealing. In the initial stage, the initialization weights and biases of ELM

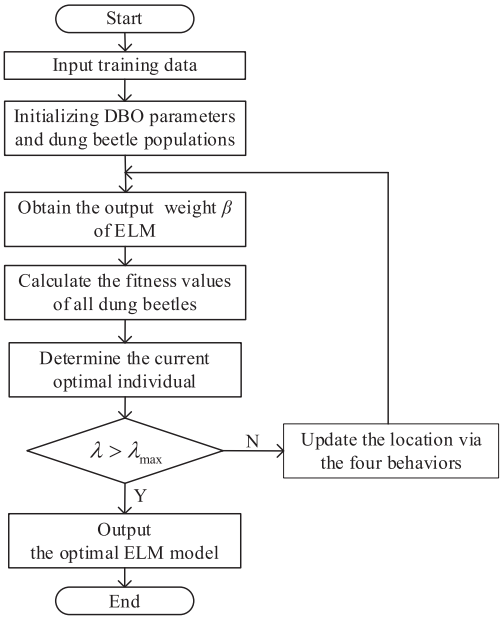

Fig. 2. Optimization process of ELM by using DBO algorithm.

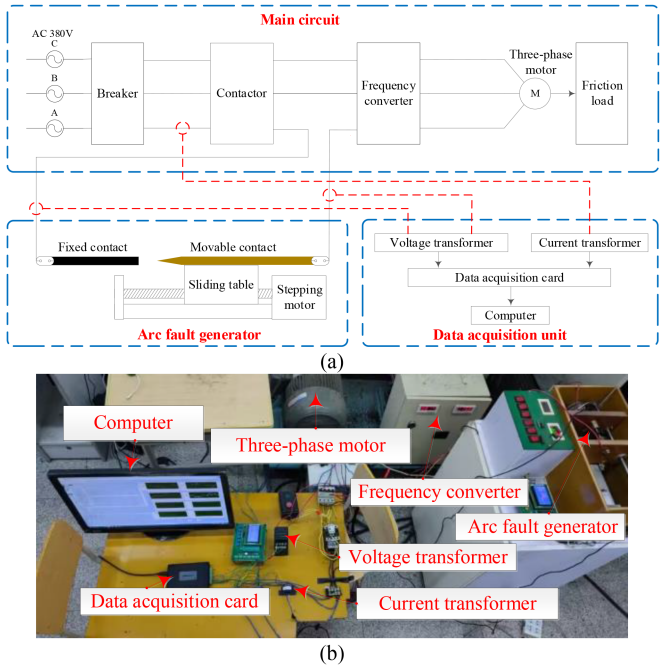

Fig. 3. Experimental platform. (a) Structure. (b) Photo.

are randomly generated, and the mean square error (MSE) of the predicted residuals on the training set is used as the fitness function. Then, the fitness values of the populations of these four behaviors are calculated. Finally, the optimal position is updated by using these four behaviors.

The MSE can be calculated as

$$\mathrm{MSE} = \frac{1}{M}\sum_{i=1}^{M}(s_i - x_i)^2 \tag{5}$$

where x_i is the true value and s_i is the corresponding predicted value.

The optimization process of ELM by using DBO algorithm is shown in Fig. 2. The specific implementation steps are as follows.

Step 1: Input training sample data, and then initialize the DBO parameters and generate the initial dung beetle population. The individual dung beetles are the initial input weight and the hidden layer bias of the ELM.

Step 2: Build the ELM prediction model. That is, calculate the output weight by using the training data and the generalized inverse matrix theory.

Step 3: Calculate the residual MSE of the ELM prediction model for all dung beetles, and use it as the fitness function of the optimization.

Step 4: According to the fitness, determine the current optimal individual, i.e., the optimal input weight and hidden layer bias of the ELM.

Step 5: Check whether the number of iterations λ is greater than the maximum number of iterations $\lambda_{\max}$. If so, output the optimal ELM prediction model. Otherwise, update the location via the four behaviors, and then repeat steps 2–5.

III. Experimental Verification

A. Experimental Platform and Experimental Scheme

The SAF experimental platform is shown in Fig. 3. A three-phase commercial power supply was used as the experimental power supply of the main circuit of the platform. Its rated output voltage is ac 380V, and its rated output frequency is 50 Hz. A VFD110E43A type frequency converter and a Y160M-6-11kW type three-phase asynchronous motor were used as the experimental load. The experimental current of the circuit can be obtained by adjusting a friction load driven by the three-phase motor. An arc fault generator was connected in series at the front end of the frequency converter in the A-phase circuit. A flat carbon rod and a pointed copper rod were respectively used as the fixed and movable contacts of the arc fault generator. By controlling the stepper motor installed in the arc fault generator, the movable and fixed contacts can be separated so as to generate a SAF.

During the experiment, the operation current of the main circuit and arc voltage were respectively collected by using a LHB100A5VY2 type current transformer and a LHB-T1 voltage transformer. The data were collected and uploaded to a computer by using a USB3200 type data acquisition card. And then they were displayed and stored by using a self-developed signal process program. In this article, the current signal was used to detect the SAF, while the arc voltage signal was only used to determine the working state of the circuit so as to evaluate whether the detection result given by the detection method is correct or not.

The experimental scheme is given in Table I. The experiments were conducted under room temperature and humidity conditions. The data sampling frequency was set to 10 kHz. The load

TABLE I
EXPERIMENTAL SCHEME

Group No.	Power supply	Current (A)	Working state
1	Commercial power supply	12	Normal
2	Commercial power supply	12	Fault

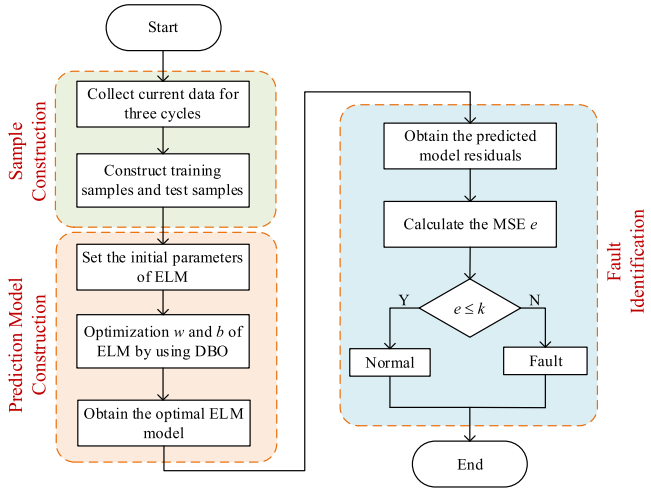

Fig. 4. Overall process of the SAF detection method.

current of the frequency converter was adjusted to 12 A. The carrier frequency and the operating frequency of the frequency converter were set to 8 kHz and 50 Hz, respectively. There are two experimental states, that is, normal state and fault state. In normal state, the movable and fixed contacts of the arc fault generator are in good contact to simulate the normal working state of the circuit. In fault state, generating an arc discharge in the contact gap of the arc fault generator to simulate the SAF in the circuit. The specific method is as follows. Make the movable contact and the static contact separate by controlling the movement of the movable contact. Once a small gap between the two contacts is formed, the gas gap will be broken down, resulting in an arc discharge. At this time, stop moving the movable contact to keep the arc burning steadily.

B. SAF Detection Method

The overall process of the SAF detection method is shown in Fig. 4. It mainly includes three steps, that is, sample construction, prediction model construction and fault identification. The detailed process is stated as follows:

Step 1. Sample Construction: Three cycle current signals were intercepted from the experimental data samples, with a total of 600 sampling points. They were labeled as $X = [x_1, x_2, \cdots, x_{600}]$. The construction method is shown in Fig. 5. The first to 400th sampling data were used to construct 200 training samples. Each 200 consecutive sampling data were taken as the input vector of a training sample, and the next sampling data was taken as the output of the training sample. The 201st to 600th sampling data were used to construct 200 test samples. Similarly, each 200 consecutive sampling data were taken as the input vector of a test sample, and the next sampling data was taken as the expected output of the test sample.

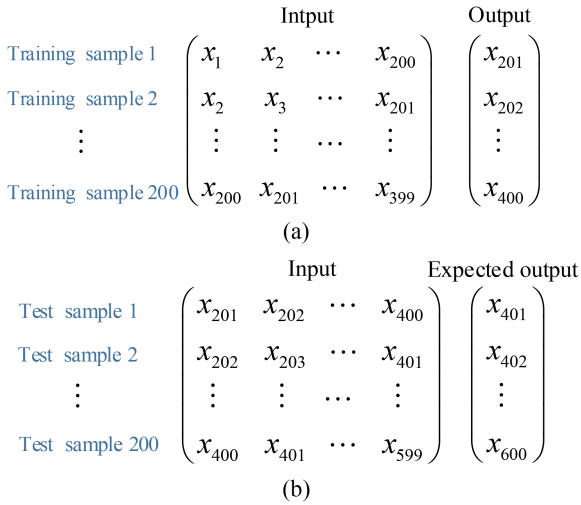

Fig. 5. Sample construction method. (a) Training samples. (b) Test samples.

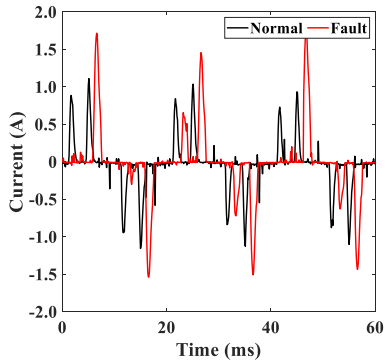

Fig. 6. Measured current waveform.

Step 2. Prediction Model Construction: The DBO-ELM prediction model was constructed with the created 200 training samples. The DBO population size was set to 20, the maximum number of iterations $\lambda_{\max}$ was set to 20, and the optimization range of the parameters ranged from -1 to 1. The number of hidden layer neurons in ELM was set to 70, and the activation function was Sigmoid. The specific construction method and parameter optimization process are shown in Figs. 1 and 2.

Step 3. Fault Identification: The test samples were input into the DBO-ELM prediction model and the prediction results of the model were obtained. The predicted residual MSE e of the model was calculated by using the predicted results and expected output results. A uniform threshold k was used to judge whether there is a SAF or not in the circuit.

C. Detection Results Analysis

The measured current waveform in the experiment is shown in Fig. 6. Since the ratio between the output signal of the current transformer and the actual current signal is 1:20, the actual current amplitude is 20 times of the measured current waveform. The frequency converter belongs to a nonlinear load, and the normal current waveform exhibits a bimodal characteristic. When a SAF occurs, there are phenomena, such as the

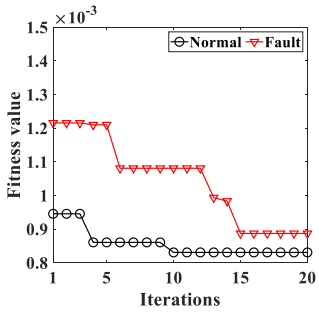

Fig. 7. Fitness curve.

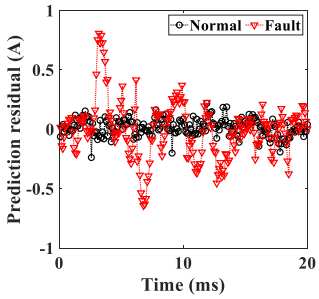

Fig. 8. Predicted residual.

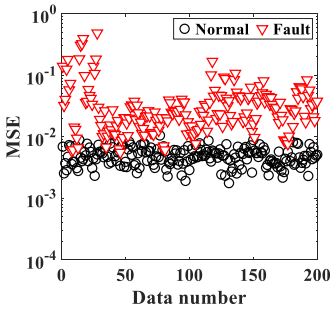

Fig. 9. MSE of the predicted residuals.

amplitude difference change of the double peaks and increasing of the burrs in the current.

Based on the established DBO-ELM prediction model, the fitness curve of the DBO optimization process and the prediction residual of the third cycle of the current data in Fig. 6 were obtained, as shown in Figs. 7 and 8, respectively. When a SAF occurs, the overall prediction residual of the model shows an increasing trend, which is consistent with the theoretical analysis in Introduction.

In order to analyze the prediction results of the DBO-ELM, 200 segments of current data in normal working state and 200 segments of current data in SAF working state were intercepted respectively, and each segment of the current data was three cycles. The MSE e of the predicted residual for each section of current data and the indicator R^2 were calculated by using the detection method in Section III-B. The calculation results are shown in Figs. 9 and 10. The indicator R^2 can be calculated as

$$R^2 = 1 - \frac{\sum_{i=1}^{M} (x_i - s_i)^2 / M}{\sum_{i=1}^{M} (x_i - \bar{x})^2 / M} \tag{6}$$

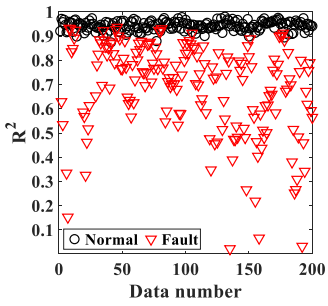

Fig. 10. R^2 of the predicted results.

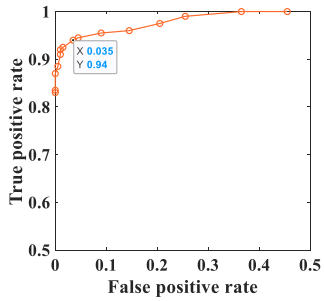

Fig. 11. ROC curve.

where x_i is the true value, s_i is the corresponding predicted value, and $\bar{x}$ is the mean of the true values.

The smaller the MSE of the prediction residual and the closer the R^2 is to 1, the more accurate the prediction result is. As seen in Figs. 9 and 10, the current prediction results of the DBO-ELM model are very accurate in normal state. When the SAF arc occurs, due to the increase of unpredictability in the current signal, the MSE of the predicted residuals of the DBO-ELM model increases significantly, and the R^2 deviates by 1. So it is possible to distinguish whether a SAF occurs in the circuit by predicting the MSE combined with a threshold.

To determine the fault threshold k, the receiver operating characteristic (ROC) curve was used to optimize the threshold. The ROC curve is the connection curve of the corresponding coordinates of true positive rate and false positive rate under different thresholds. Wan et al. [35] pointed out that the recognition accuracy of the point closest to the coordinate (0,1) on the ROC curve is the highest. So, the threshold corresponding to the point closest to the coordinate of (0,1) on the curve was set as the optimal threshold. The threshold was set in the range of 0.005–0.011 and increased by the step of 0.0005. The true positive rate and false positive rate of the data in Fig. 9 were counted, and the ROC curve was drawn, as shown in Fig. 11. The distance between the points on the ROC curve corresponding to different thresholds and the coordinate (0,1) was further calculated, as shown in Fig. 12. As seen in Fig. 12, the distance between the coordinate (0,1) and the point on the ROC curve corresponding to threshold $k = 0.0085$ is the shortest. So the threshold k was set to 0.0085. In this case, the true positive rate and false positive rate are 0.94 and 0.035, respectively. The detection results of the SAF under this threshold were statistically obtained, as shown

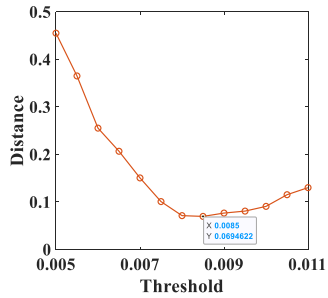

Fig. 12. Distance from the coordinates (0,1).

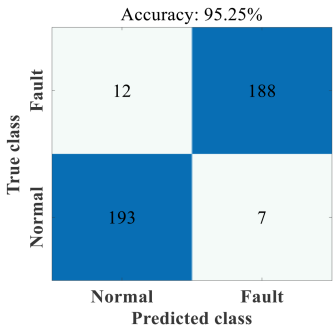

Fig. 13. Detection results.

TABLE II
HARMONIC PARAMETERS OF POWER SUPPLY U_1-U_4

Order of harmonics	U_1	U_2	U_3	U_4
3	1.1%/0°	2.2%/0°	4.9%/0°	3.0%/180°
5	2.8%/0°	5.6%/0°	1.6%/0°	2.75%/0°
7	1.4%/0°	2.8%/0°	2.7%/0°	2.40%/180°
9	2.3%/0°	4.6%/0°	0.0%/0°	2.0%/0°
11	1.5%/0°	3.0%/0°	1.4%/0°	1.4%/180°
13	0.0%/0°	0.0%/0°	0.0%/0°	0.8%/0°
15	0.0%/0°	1.4%/0°	2.0%/0°	0.0%/0°
17	0.0%/0°	0.0%/0°	1.1%/0°	0.0%/0°
21	0.0%/0°	1.0%/0°	0.0%/0°	0.0%/0°

in Fig. 13. It shows that the detection accuracy of the method for the SAF in the frequency converter load circuit is 95.25%.

IV. PERFORMANCE ANALYSIS OF THE PROPOSED DETECTION METHOD UNDER UNKNOWN WORKING CONDITIONS

A. Performance Analysis of the Method Under Unknown Power Harmonic Conditions

In the industrial field, the power quality of power supply is poor and the harmonic content is complex and variable. In order to test the detection performance of the method under unknown power harmonic conditions, the SAF experiments under four groups of power harmonic parameter (i.e., harmonic power supply U_1-U_4) conditions were conducted. A Chroma 6590 type programmable ac power supply was used to output the power supply with different harmonic parameters. The programmable power supply was connected between the circuit breaker and the contactor of the experimental platform in Fig. 3. The harmonic parameters (i.e., harmonic content and phase angle) of the harmonic power supply U_1-U_4 are given in Table II. A total of

TABLE III
SAF EXPERIMENTAL SCHEME IN SECTION IV-A

Group No.	Working state	Harmonic power supply
1-2	Normal, Fault	U_1
3-4	Normal, Fault	U_2
5-6	Normal, Fault	U_3
7-8	Normal, Fault	U_4

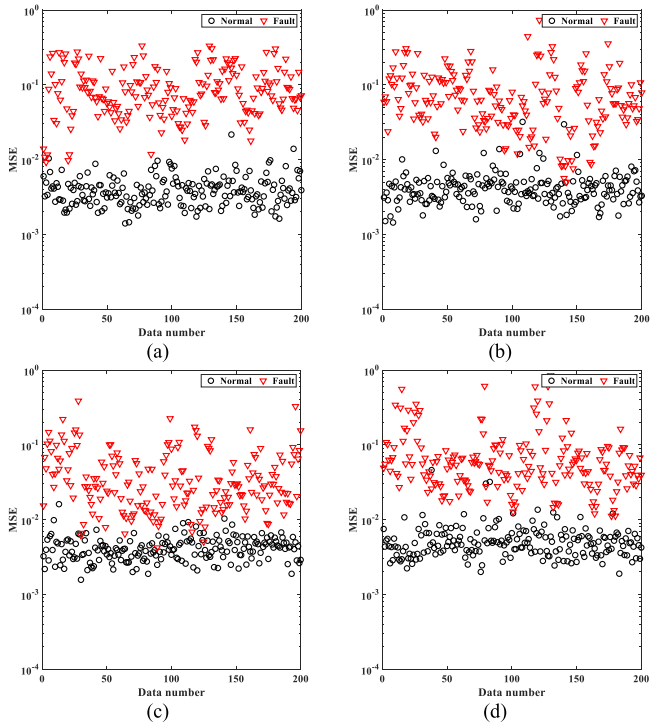

Fig. 14. MSE of the predicted residuals under different harmonic power supply conditions. (a) U_1. (b) U_2. (c) U_3. (d) U_4.

eight experiments were conducted and the experimental scheme is given in Table III.

For each group of the SAF experiments, 200 segments of current data were intercepted and the MSE of the predicted residual of each current data were calculated by using the method in Section III-B. The calculation results are shown in Fig. 14. When the uniform threshold k was set to 0.0085, both the normal state and the SAF state of the circuit with the harmonic power supply can still be distinguished. As shown in Fig. 15, the detection accuracy of the SAF under four kinds of harmonic power supply conditions is higher than 95%. It verifies that the proposed method can accurately detect the SAF under the unknown power harmonic conditions.

B. Performance Analysis of the Method Under the Conditions of Unknown Operating Parameters of Frequency Converter

In the industrial field, the two operating parameters of the frequency converter, that is, carrier frequency and operating frequency, will be adjusted or changed according to the actual situation. In order to test the detection performance of the proposed method under the conditions of unknown operating parameters of the frequency converter, the SAF experiments under different carrier frequencies and operating frequencies

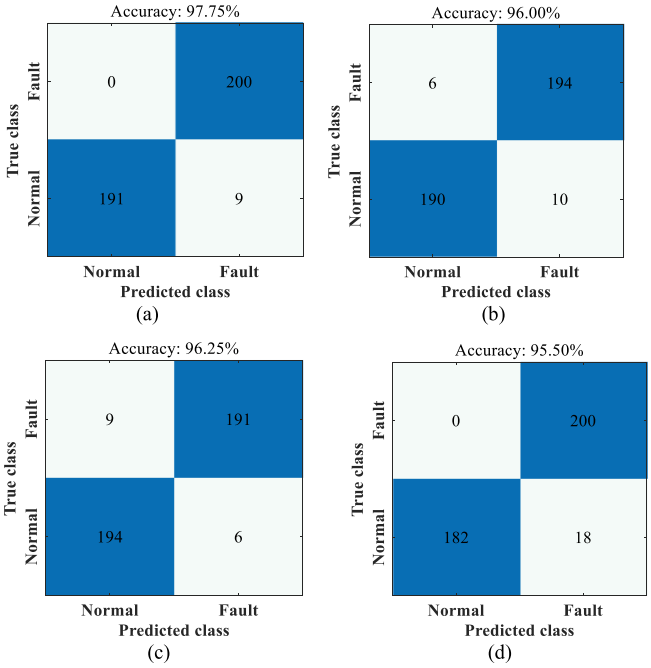

Fig. 15. Detection results under different harmonic power supply conditions. (a) U_1. (b) U_2. (c) U_3. (d) U_4.

TABLE IV
SAF EXPERIMENTAL SCHEME IN SECTION IV-B

Group No.	Working state	Carrier frequency (kHz)	Operation frequency (Hz)
1-2	Normal, Fault	3	50
3-4	Normal, Fault	13	50
5-6	Normal, Fault	8	40
7-8	Normal, Fault	8	45

conditions were carried out with the commercial power supply. The specific experimental scheme is given in Table IV.

The MSE of the predicted residuals and the detection results of the SAF were calculated with the method in Section IV-A, as shown in Figs. 16 and 17, respectively. Fig. 17 shows that the detection accuracy of the SAF is higher than 91% even when the frequency converter operates in different working states. It verifies that the proposed method can accurately detect the SAF under the unknown conditions of different operating parameters of the frequency converter.

C. Performance Analysis of the Method Under Unknown Current Conditions

The current of the three-phase frequency converter load circuit will fluctuate with the vary of the driven load of the motor. In order to test the detection performance of the proposed method under unknown current conditions, the SAF experiments under different current conditions were carried out by adjusting the frictional load in the experimental platform in Fig. 3. The specific experimental scheme is given in Table V. Where, the fluctuation means that the current fluctuates within the range of 15–20 A.

The MSE of the predicted residuals and the detection results of the SAF were calculated with the method in Section IV-A, as

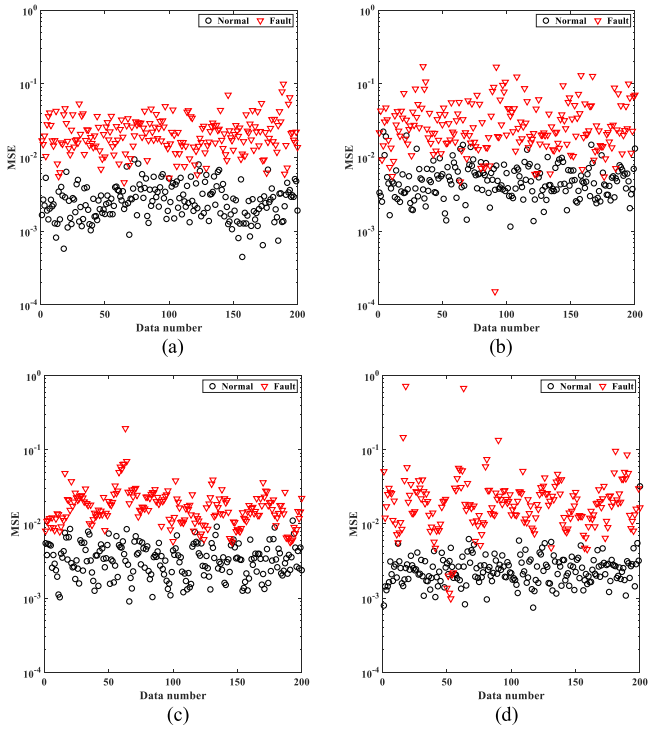

Fig. 16. MSE of the predicted residuals under the conditions of different operating parameters of the frequency converter. (a) Group no. 1-2. (b) Group no. 3-4. (c) Group no. 5-6. (d) Group no. 7-8.

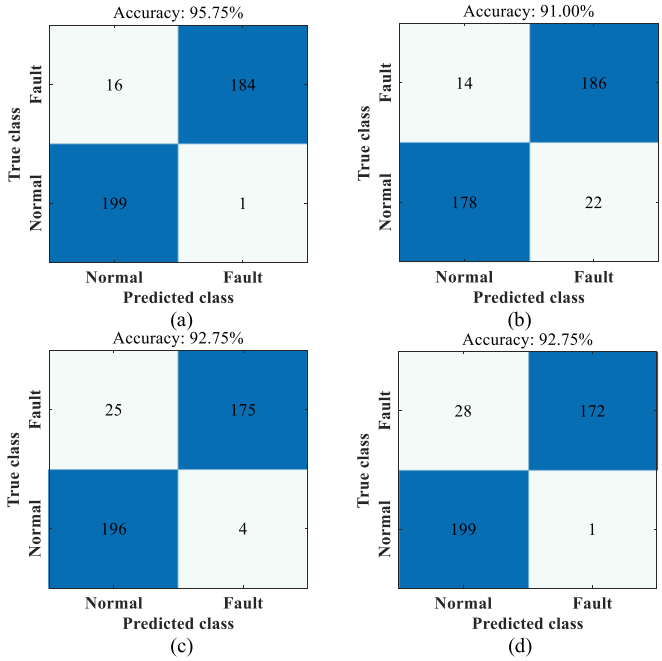

Fig. 17. Detection results under the conditions of different operating parameters of the frequency converter. (a) Group no. 1-2. (b) Group no. 3-4. (c) Group no. 5-6. (d) Group no. 7-8.

TABLE V
SAF EXPERIMENTAL SCHEME IN SECTION IV-C

Group No.	Working state	Current (A)
1-2	Normal, Fault	15
3-4	Normal, Fault	18
5-6	Normal, Fault	20
7-8	Normal, Fault	Fluctuation

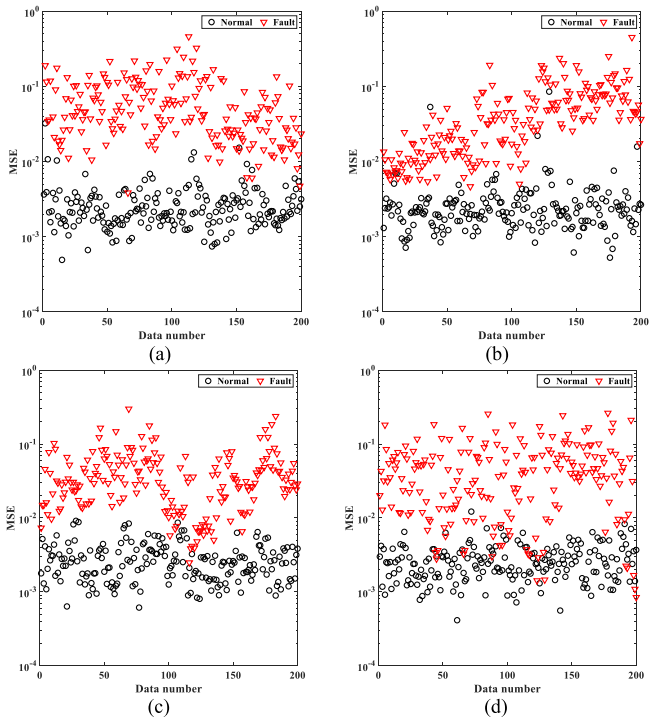

Fig. 18. MSE of the predicted residuals under different current conditions. (a) 15A. (b) 18A. (c) 20A. (d) Fluctuation.

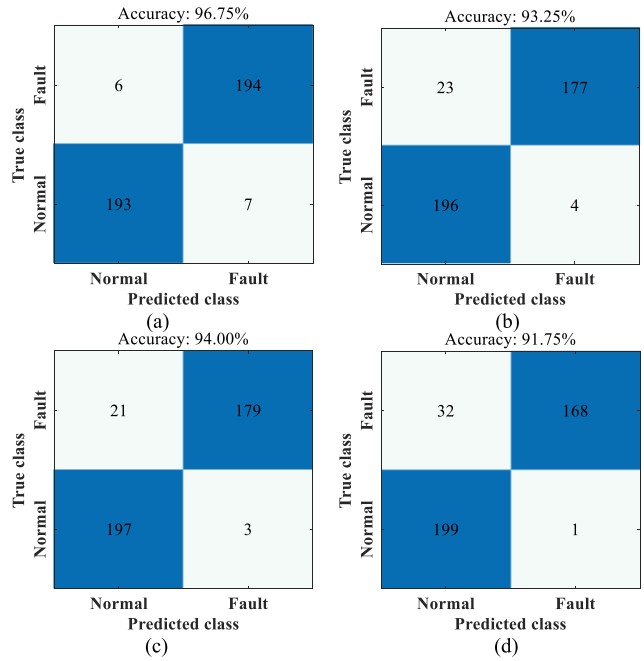

Fig. 19. Detection results under different current conditions. (a) 15A. (b) 18A. (c) 20A. (d) Fluctuation.

shown in Figs. 18 and 19, respectively. Fig. 19 shows that the detection accuracy of the SAF is higher than 91% under different current conditions. It verifies that the proposed method can accurately detect the SAF under the unknown current conditions.

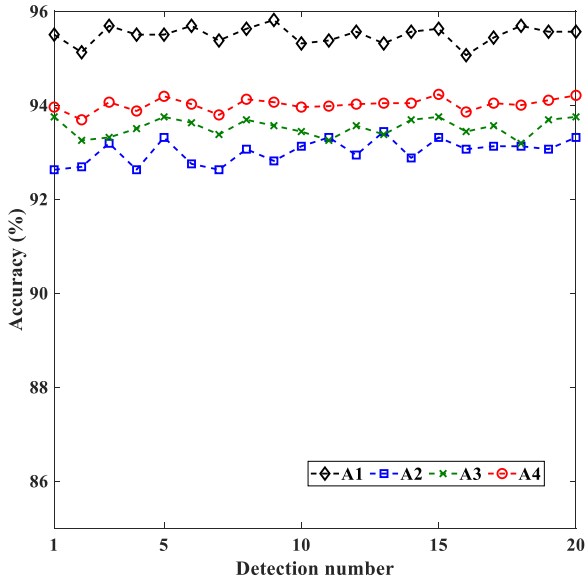

Fig. 20. Detection results of the SAF with 20 repetitions.

D. Stability Analysis of DBO-ELM Prediction Model

DBO belongs to heuristic algorithm. When optimizing ELM, there will be uncertain optimization results, which will affect the stability of the SAF detection results.

In order to evaluate the stability of the DBO-ELM prediction model, 20 repeat tests were carried out with the experimental data in Section IV-A–C, respectively.

The average detection accuracy per detection of the SAF under the conditions of unknown power supply harmonics, unknown frequency converter operating parameters, and unknown current was *A1*, *A2* and *A3*, respectively. The average value of *A1*, *A2* and *A3* was calculated, labeled as *A4*. The detection results are shown in Fig. 20. As shown in Fig. 20, among the 20 repeat tests, the difference between the maximum and minimum detection accuracy under the same working condition is less than 1%. It indicates that the DBO-ELM prediction model has good stability.

E. Detection Results of the SAF in B-Phase or C-Phase Circuit

In order to test whether the proposed method can detect the SAFs occurred in B-phase or C-phase circuit by analyzing the measured A-phase current signal, additional SAF experiments were performed.

On the basis of the experimental platform in Fig. 3 and the experimental conditions in Table I, the arc fault generator was connected in B-phase and C-phase circuits, respectively, and the SAF experiments were carried out. 200 segments of current data were intercepted respectively from the measured A-phase current signals when the SAF occurred in B-phase and C-phase circuits. And the MSE of the predicted residuals was calculated, as shown in Fig. 21. For the 200 SAFs occurred respectively in B-phase and C-phase circuits, there are 179 and 198 SAFs were successfully detected with the threshold of 0.0085. It verifies that the proposed method can effectively detect the SAF occurred in

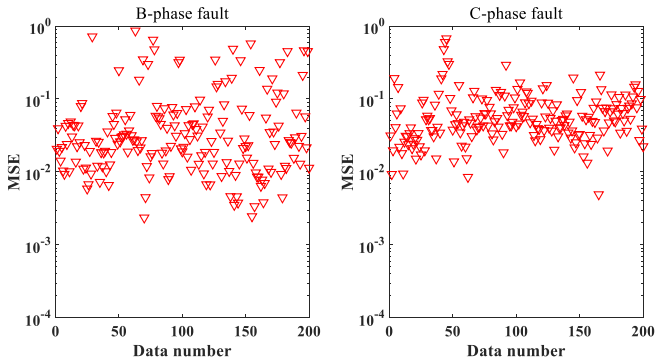

Fig. 21. MSE of the predicted residuals for the SAFs occurred in B-phase or C-phase circuit.

B-phase or C-phase circuit by analyzing the A-phase current signal.

F. Performance Analysis of Different Methods Under Unknown Working Conditions

1) Comparison of Different SAF Detection Methods: In order to verify the superiority of the proposed method in detecting the SAF under unknown working conditions, the SAF detection accuracy was tested by using four existing SAF detection methods under the conditions of different power harmonics, operating parameters of the frequency converter and current. The selected four detection methods were introduced in brief as follows.

1) *Detection Method in [2]:* The waveform difference signal between adjacent cycles of the current signal was calculated, and the amplitude was extracted as the fault feature after denoising by wavelet threshold. Then, a fixed threshold of 0.3 was used to detect the SAF.
2) *Detection Method in [36]:* Wavelet transform was performed on half cycle of the current signal, and a Hankel matrix was constructed by using wavelet coefficients. The average, root mean square (RMS), and standard deviation of the singular values of the matrix were calculated and used as feature parameters. The ratio of the feature parameters of the first half cycle to those of the second half cycle was used as a criterion, and then a threshold was used to detect the SAF.
3) *Detection Method in* [25]: Two cycles of the current signals were extracted and normalized by using the RMS of the current signal. Then, the processed signal was decomposed into five layers by EWT, and a reconstructed attractor track matrix of each decomposed signal was established. The first two singular values of each attractor track matrix were selected and used as the fault features. Finally, a SVM optimized by grid search and particle swarm optimization (PSO) was used to detect the SAF.
4) *Detection Method in [27]:* The current signal was decomposed by VMD and the intrinsic mode function (IMF) components in the frequency band between 0 and 650 Hz were obtained. Then the sample entropy and energy entropy of these IMFs were calculated and used as the fault features, and a SVM optimized by the firefly algorithm was used to detect the SAF.

TABLE VI
DETECTION RESULTS OF THE SAF UNDER UNKNOWN WORKING CONDITIONS BY USING DIFFERENT DETECTION METHODS

SAF Detection Method	*A1*/%	*A2*/%	*A3*/%	*A4*/%
In [2]	84.19	88.06	79.19	83.81
In [36]	63.94	60.12	59.31	61.12
In [25]	85.75	77.06	96.44	86.42
In [27]	50.00	80.38	68.50	66.29
Proposed in this article	96.38	93.06	93.94	94.46

The detection accuracy of the SAF under the conditions of unknown power harmonics, operating parameters of the frequency converter and current were tested with the experimental data in Section IV-A–C by using the above-mentioned four detection methods and the proposed detection method in this article. Here, the thresholds in [2] and [36] were reset by using the experimental data in Section III-C. The SVMs used in [25] and [27] were trained by using the experimental data in Section III-C.

The detection results of the SAF under unknown working conditions by using different detection methods are given in Table VI. Except for the proposed method, only the detection method in [25] has a detection accuracy of over 90% in detecting the SAF under unknown current conditions. It verifies the superiority of the proposed method in the SAF detection under unknown working conditions.

For the detection methods in [2] and [36], the extracted fault features will fluctuate when the current signal varies, caused by the change of the working condition. So, the detection accuracy of the SAF detection methods based on the threshold will be affected and lowered under unknown working conditions. The lack of experimental data under unknown working conditions in the training sample is the main reason for the decrease of detection accuracy of the detection methods in [25] and [27]. However, there are few actual SAF samples in practical engineering applications. It is very difficult to obtain a large number of training samples under different working conditions. Therefore, it is difficult for the above-mentioned four detection methods to accurately detect the SAF under unknown working conditions.

2) Comparison of Different Optimization Methods: In order to verify the superiority of the DBO algorithm in optimizing ELM, the performance of ELM optimized by other six different optimization algorithms was tested under the experimental conditions of this article. The selected six optimization methods are genetic algorithm (GA), grey wolf optimization (GWO), PSO, whale optimization algorithm (WOA), grasshopper optimization algorithm (GOA), and sparrow search algorithm (SSA), respectively.

The fitness curves of the six optimization methods were calculated by applying the data and test method used in Fig. 7, as shown in Fig. 22. According to Figs. 22 and 7, the optimal fitness values of both the six optimization methods and the DBO method were obtained, as given in Table VII. Among the seven optimization methods, the optimal fitness value of the DBO algorithm is the lowest in both normal and fault state.

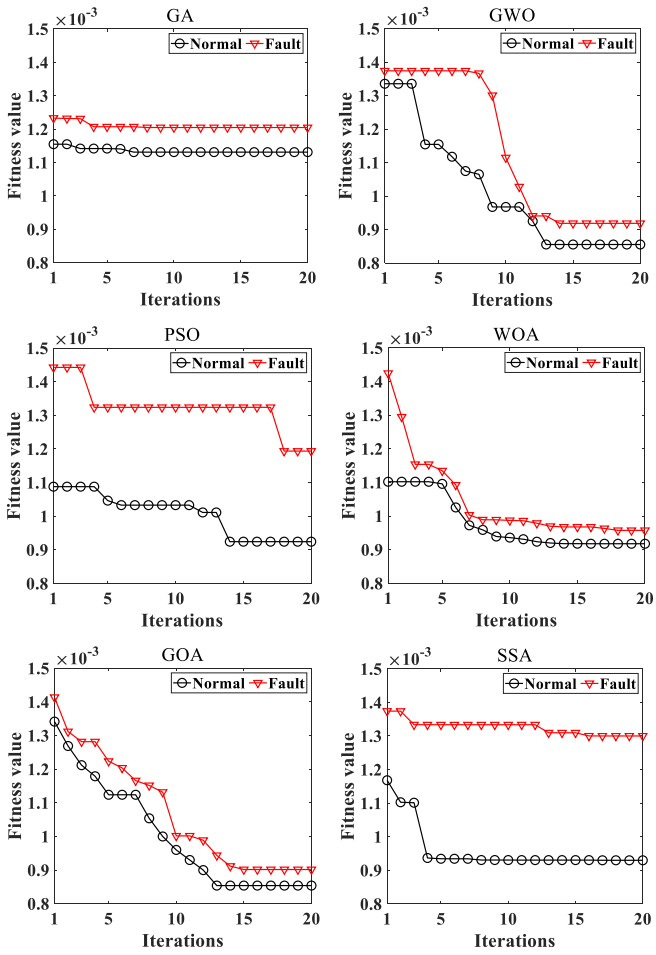

Fig. 22. Fitness curves of different optimization methods.

TABLE VII
OPTIMAL FITNESS VALUES FOR DIFFERENT OPTIMIZATION METHODS

Optimization methods	Optimal fitness values	
	Normal state	Fault state
GA	1.13×10^{-3}	1.20×10^{-3}
GWO	8.55×10^{-4}	9.18×10^{-4}
PSO	9.24×10^{-4}	1.19×10^{-3}
WOA	9.18×10^{-4}	9.57×10^{-4}
GOA	8.54×10^{-4}	9.02×10^{-4}
SSA	9.30×10^{-4}	1.30×10^{-3}
DBO	8.31×10^{-4}	8.87×10^{-4}

It indicates that the DBO algorithm has the best optimization action on ELM.

The DBO algorithm in the proposed method was replaced by GA, GWO, PSO, WOA, GOA, and SSA algorithm, respectively, and the threshold value of each method was reset according to the method in Section III-C.

The stability of the arc fault detection results discussed in Section IV-D may exist when using the above heuristic optimization algorithms. To better compare the detection accuracy of different optimization methods, 20 repeated tests were conducted for each method under three unknown working conditions, and the detection accuracy of the SAF was calculated, as given

TABLE VIII
DETECTION RESULTS OF THE SAF UNDER UNKNOWN WORKING CONDITIONS BY USING DIFFERENT OPTIMIZATION METHODS

Optimization methods	*B1*/%	*B2*/%	*B3*/%	*B4*/%
GA	96.79	90.56	94.03	93.79
GWO	97.18	91.25	93.15	93.86
PSO	93.25	93.38	95.19	93.94
WOA	92.67	92.90	90.03	91.87
GOA	96.92	90.54	94.41	93.96
SSA	94.84	92.28	92.04	93.05
DBO	95.49	93.02	94.25	94.25

TABLE IX
DETECTION RESULTS OF THE SAF UNDER UNKNOWN WORKING CONDITIONS BY USING DIFFERENT PREDICTION MODELS

Prediction models	*A1*/%	*A2*/%	*A3*/%	*A4*/%
BP	92.75	82.62	93.19	89.52
DBO-SVR	84.56	88.69	81.25	84.83
CNN	61.31	75.19	51.44	62.65
LSTM	73.06	49.88	80.94	67.96
Proposed in this article	96.38	93.06	93.94	94.46

in Table VIII. In Table VIII, *B1*, *B2,* and *B3* are the average detection accuracy of 20 repeated tests under the conditions of unknown power harmonics, operating parameters of frequency converter and current, respectively. *B4* is the average of *B1*, *B2*, and *B3*. As given in Table VIII, among these optimization algorithms, although the *B1*, *B2,* and *B3* corresponding to DBO algorithm are not the highest, the *B4* is the highest. It validates the superiority of the DBO algorithm in the proposed method of the article.

3) Comparison of Different Prediction Models: In order to verify the superiority of the DBO-ELM prediction model under the experimental conditions and data samples in this article, the detection accuracy of four prediction models, i.e., BP neural network, SVR, CNN, and LSTM, was tested under the conditions of unknown power harmonics, unknown frequency converter operating parameters and unknown current. The number of neurons in BP neural network was set to 70, which is the same as that in ELM used in this article. The penalty factor and regularization coefficient of SVR were optimized by DBO, and the method was labeled as DBO-SVR. The structure and parameters of CNN and LSTM were set according to [31] and [32]. The thresholds corresponding to these four models were adjusted according to the method in Section III-C.

Table IX gives the detection results of the SAF under unknown working conditions by using different prediction models. Although *A1* and *A3* of the BP prediction model are over 90%, the *A2* and *A4* of the DBO-ELM prediction model are still significantly higher than that of the BP prediction model. The detection accuracy of DBO-SVR, CNN and LSTM is less than 90% under three unknown conditions. It is mainly due to the small number of training samples selected in this article, which results in the poor adaptability of the deep learning-based algorithms such as CNN or LSTM to different working conditions. Based on the above analysis, the superiority of the DBO-ELM prediction model was further verified.

V. Conclusion

To detect the SAF in three-phase frequency converter load circuit under unknown working conditions, a SAF detection method based on real-time updating of ELM prediction model and utilizing the threshold of the MSE of the predicted model residual was proposed. The main conclusions are as follows.

1) The randomness and instability of the SAF will increase the unpredictability of the current signal and make the residual of the prediction model increase. The method of training and updating prediction model with real-time data can effectively deal with the variation problem of both current signal and its characteristics, which was caused by the change of working conditions. It is convenient to use predicted residuals and a uniform threshold to achieve the detection of the SAF under different working conditions. It provides a new approach for detecting the SAF under unknown working conditions.
2) A SAF detection method based on DBO-ELM prediction model and a fixed threshold was proposed. The MSE of the predicted residuals can be obtained by updating the DBO-ELM prediction model in real time. When the frequency converter load circuit works in normal state, the MSE is generally smaller than 0.0085 under different working conditions. While the MSE is generally greater than 0.0085 when a SAF occurred in the circuit. So the fault threshold was set to 0.0085. In this case, the detection accuracy is higher than 90%. Among them, the true positive rate is not lower than 0.84, and the false positive rate is not higher than 0.11. It was verified that the proposed method can accurately detect the SAF occurred in three-phase frequency converter load circuit under unknown working conditions. The proposed method provides a reference for the development of AFCI under complex working conditions.

Most of the existing SAF detection methods use fixed current signal features and identification models. When the current signal changes due to working conditions, the detection methods cannot be adjusted in time, which affects the detection results of the SAF. In this article, a new detection method of the SAF by using real-time current data to train and update the prediction model was proposed. The prediction model can be updated with the change of working conditions, which can weaken the influence of the change of working conditions on both the residual error of the prediction model and fault features, and then realize the SAF detection under unknown working conditions. Since the DBO-ELM prediction model needs to be retrained every time when it detects the SAF, it is a challenge for the detection method to be applied to commercial microprocessors. To solve this problem, the research team is focusing on the study on online sequential extreme learning machine based predictive models. It is expected to solve the issue by using new data to modify the predicted models online, rather than retraining the models, so as to lower the performance requirements of the detection method on the microprocessors.

References

[1] Z. He et al., "Identification method for low-voltage AC series arc fault,"

[2] G. Zhang et al., "Online detection method for series arc fault in low-voltage systems," *Trans. China Electrotech. Soc.*, vol. 31, no. 8, pp. 109–115, Apr. 2016.

[3] G. Artale, A. Cataliotti, V. Cosentino, D. Di Cara, S. Nuccio, and G. Tinè, "Arc fault detection method based on CZT low-frequency harmonic current analysis," *IEEE Trans. Instrum. Meas.*, vol. 66, no. 5, pp. 888–896, May 2017.

[4] H. Zhao et al., "A series arc fault detection method based on relevant theories and zero rest feature fusion," *Chin. J. Sci. Instrum.*, vol. 41, no. 4, pp. 218–228, Apr. 2020.

[5] N. Qu, J. Wang, and J. Liu, "An arc fault detection method based on current amplitude spectrum and sparse representation," *IEEE Trans. Instrum. Meas.*, vol. 68, no. 10, pp. 3785–3792, Oct. 2019.

[6] R. Jiang and Y. Zheng, "Series arc fault detection using regular signals and time-series reconstruction," *IEEE Trans. Ind. Electron.*, vol. 70, no. 2, pp. 2026–2036, Feb. 2023.

[7] J. Lezama et al., "An embedded system for AC series arc detection by inter-period correlations of current," *Elect Power Syst. Res.*, vol. 129, pp. 227–234, Dec. 2015.

[8] J. Kim, D. Neacşu, R. Ball, and B. Lehman, "Clearing series AC arc faults and avoiding false alarms using only voltage waveforms," *IEEE Trans. Power Del.*, vol. 35, no. 2, pp. 946–956, Apr. 2020.

[9] E. Calderon-Mendoza, P. Schweitzer, and S. Weber, "Kalman filter and a fuzzy logic processor for series arcing fault detection in a home electrical network," *Int. J. Elect. Power Energy Syst.*, vol. 107, pp. 251–263, May 2019.

[10] J. Siegel et al., "Real-time deep neural networks for internet-enabled arc-fault detection," *Eng. Appl. Artif. Intell.*, vol. 74, pp. 35–42, Sep. 2018.

[11] F. Ferracuti, P. Schweitzer, and A. Monteriù, "Arc fault detection and appliances classification in AC home electrical networks using recurrence quantification plots and image analysis," *Elect. Power Syst. Res.*, vol. 201, Dec. 2021, Art. no. 107503.

[12] Y. Wang, F. Zhang, and S. Zhang, "A new methodology for identifying arc fault by sparse representation and neural network," *IEEE Trans. Instrum. Meas.*, vol. 67, no. 11, pp. 2526–2537, Nov. 2018.

[13] Z. Zhang, J. Ren, X. Tang, S. Jing, and W.-J. Lee, "Novel approach for arc fault identification with transient and steady state based time-frequency analysis," *IEEE Trans. Ind. Appl.*, vol. 58, no. 4, pp. 4359–4369, Jul./Aug. 2022.

[14] Y. Wang, L. Hou, K. C. Paul, Y. Ban, C. Chen, and T. Zhao, "ArcNet: Series AC arc fault detection based on raw current and convolutional neural network," *IEEE Trans. Ind. Inform.*, vol. 18, no. 1, pp. 77–86, Jan. 2022.

[15] Y. Wang, F. Zhang, X. Zhang, and S. Zhang, "Series AC arc fault detection method based on hybrid time and frequency analysis and fully connected neural network," *IEEE Trans. Ind. Inform.*, vol. 15, no. 12, pp. 6210–6219, Dec. 2019.

[16] Q. Yu, G. Huang, and Y. Yang, "Low voltage AC series arc fault detection method based on parallel deep convolutional neural network," *IOP Conf. Ser., Mater. Sci. Eng.*, vol. 490, no. 7, May 2019, Art. no. 072020.

[17] R. Jiang, Y. Wang, X. Gao, G. Bao, Q. Hong, and C. D. Booth, "AC series arc fault detection based on RLC arc model and convolutional neural network," *IEEE Sensors J*, vol. 23, no. 13, pp. 14618–14627, Jul. 2023.

[18] R. Ding et al., "Identification of AC series arc fault based on adjacent wave current difference and randomness," *Power Syst. Protection*, vol. 51, no. 8, pp. 169–178, Apr. 2023.

[19] Q. Gong et al., "A method for identifying AC series arc fault based on arc randomness and convolutional networks," *Power Syst. Autom.*, vol. 46, no. 24, pp. 162–169, Apr. 2022.

[20] Y. Wang et al., "Arc fault detection based on empirical wavelet transform composite entropy and feature fusion," *Grid Tech.*, vol. 47, no. 5, pp. 1912–1919, May 2023.

[21] G. Rocha, L. Pulz, and D. Gazzana, "Serial arc fault detection through wavelet transform and support vector machine," in *Proc. IEEE Int. Conf. Environ. Elect. Eng. IEEE Ind. Commercial Power Syst. Eur.*, 2021, pp. 1–5.

[22] A. Gupta, A. Routray, and V. Naikan, "Series arc fault detection in low voltage distribution system with signal processing and machine learning approach," in *Proc. 47th Annu. Conf. IEEE Ind. Electron. Soc.*, 2021, pp. 1–6.

[23] J. Duan, L. Zeng, Y. Wu, L. Chen, and C. L. P. Chen, "BroadNet: A novel broad learning system based series AC arc fault detection approach with zero phase component analysis whitening transformation," *IEEE Sensors J.*, to be published, doi: 10.1109/JSEN.2024.3373598.

[24] C. Han, Z. Wang, A. Tang, H. Gao, and F. Guo, "Recognition method of AC series arc fault characteristics under complicated harmonic conditions,"

[25] H. Gao, Z. Wang, C. Han, A. Tang, F. Guo, and B. Li, "Feature extraction method of series arc fault occurred in three-phase motor with inverter circuit," *IEEE Trans. Power Electron.*, vol. 37, no. 9, pp. 11164–11173, Sep. 2022.
[26] Z. Wang, S. Tian, H. Gao, C. Han, and F. Guo, "An on-line detection method and device of series arc fault based on lightweight CNN," *IEEE Trans. Ind. Inform.*, vol. 19, no. 10, pp. 9991–10003, Oct. 2023.
[27] Z. Wang, C. Han, H. Gao, and F. Guo, "Identification of series arc fault occurred in the three-phase motor with frequency converter load circuit via VMD and entropy-based features," *IEEE Sensors J.*, vol. 22, no. 24, pp. 24320–24332, Dec. 2022.
[28] Y. Liu, Z. Lv, S. Zhang, L. Zhang, and F. Guo, "Feature extraction and detection method of series arc faults in a motor with inverter circuits under vibration conditions," *IEEE Trans. Ind. Electron.*, vol. 71, no. 6, pp. 6294–6303, Jun. 2024, doi: 10.1109/TIE.2023.3294630.
[29] G. Li et al., "Ultra short-term power load forecasting based on randomly distributive embedded framework and BP neural network," *Power Syst. Technol.*, vol. 44, no. 2, pp. 437–445, Feb. 2020.
[30] J. Xu, Y. Ni, and C. Zhu, "Remaining useful life prediction for lithium-ion batteries based on improved support vector regression," *Trans. China Electrotech. Soc.*, vol. 36, no. 17, pp. 3693–3704, Sep. 2021.
[31] X. Dong, L. Qian, and L. Huang, "A CNN based bagging learning approach to short-term load forecasting in smart grid," in *Proc. IEEE SmartWorld, Ubiquitous Intell. Comput., Adv. Trusted Computed, Scalable Comput. Commun., Cloud Big Data Comput., Internet People Smart City Innov.*, 2017, pp. 1–6.
[32] W. Kong, Z. Dong, D. J. Hill, F. Luo, and Y. Xu, "Short-term residential load forecasting based on resident behaviour learning," *IEEE Trans. Power Syst.*, vol. 33, no. 1, pp. 1087–1088, Jan. 2018.
[33] S. Zhang, Z. Liu, X. Huang, and W. Xiao, "A modified residual extreme learning machine algorithm and its application," *IEEE Access*, vol. 6, pp. 62215–62223, Oct. 2018.
[34] J. Xue and B. Shen, "Dung beetle optimizer: A new meta-heuristic algorithm for global optimization," *J. Supercomputing*, vol. 79, no. 7, pp. 1–32, May 2023.
[35] P. Wan et al., "On-road experimental study on driving anger identification model based on physiological features by ROC curve analysis," *IET Intell. Transport Syst.*, vol. 11, no. 5, pp. 290–298, Mar. 2017.
[36] Q. Lu et al., "Series arc fault detection method based on wavelet transform and singular value decomposition," *Trans. China Electrotech. Soc.*, vol. 32, no. 17, pp. 208–217, Sep. 2017.

Hongxin Gao (Member, IEEE) received the B.S., M.S., and Ph.D. degrees in electrical engineering from Liaoning Technical University, Huludao, China, in 2013, 2015, and 2019, respectively.

He is currently an Associate Professor with Liaoning Technical University. His current research interests include electrical contact, electric arc, and intelligent electrical apparatus.

Kunyuan Wang received the B.S. degree in electrical engineering in 2022 from Liaoning Technical University, Huludao, China, where he is currently working toward the M.S. degree in electrical engineering.

His current research interests include electrical contact and electric arc.

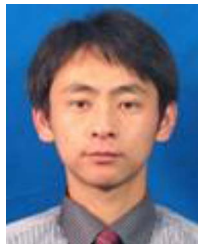

Zhiyong Wang (Member, IEEE) received the B.S. and M.S. degrees in electrical engineering and the Ph.D. degree in safety management engineering from Liaoning Technical University, Huludao, China, in 2005, 2008, and 2017, respectively.

He is currently an Associate Professor with Liaoning Technical University. His current research interests include electrical contact, electric arc, and intelligent electrical apparatus.

Jiacheng Cai received the B.S. degree in electrical engineering from Liaoning Technical University, Huludao, China, in 2013, and the M.S. degree in control engineering from Northeast Electric Power University, Jilin, China, in 2016. He is currently working toward the Ph.D. degree in electrical engineering.

He is currently a Lecturer with Liaoning Technical University. His current research interests include electrical contact and electric arc.

Yuze Lv received the B.S. degree in electrical engineering in 2023 from Liaoning Technical University, Huludao, China, where he is currently working toward the M.S. degree in electrical engineering.

His current research interests include electrical contact and electric.